Optical properties of Mg-based II-VI ternaries and quaternaries: $Cd_{1-x}Mg_xTe$ and $Cd_{1-x-y}Mg_xMn_yTe$

Eunsoon Oh, C. Parks, I. Miotkowski, M. Dean Sciacca, A. J. Mayur, and A. K. Ramdas
Department of Physics, Purdue University, West Lafayette, Indiana 47907-1396
(Received 11 June 1993)

We have investigated the photoluminescence, Raman, and infrared spectra of $Cd_{1-x}Mg_xTe$ and $Cd_{1-x-y}Mg_xMn_yTe$ bulk crystals with the zinc-blende structure. From the band-gap (E_g) photoluminescence peak we deduce $E_g = 1.595 + 1.607x + 1.592y$ eV at 10 K. The Raman spectra of the quaternary alloys exhibit a classic three-mode behavior with MgTe-like, MnTe-like, and CdTe-like LO-TO pairs of zone-center optical phonons, in decreasing order of frequency. Their composition dependence follows the modified random-element isodisplacement model. For very small x and/or y, the infrared absorption spectra recorded with a Fourier-transform spectrometer clearly reveal the local modes of Mn^{2+} and Mg^{2+}. Mn^{2+} exhibits one and Mg^{2+} three local modes corresponding to their isotopic abundances; the latter have frequencies proportional to $1/\sqrt{M_{Mg^{2+}}}$.

I. INTRODUCTION

The Mg-based II-VI ternaries and quaternaries such as $Cd_{1-x}Mg_xTe$ (Ref. 1) and $Zn_{1-x}Mg_xSe_{1-y}S_y$,[2] in which a fraction of the group II elements are replaced by Mg, have interesting physical properties. Besides being of fundamental interest, their importance for potentially useful optoelectronic devices has recently attracted attention.[3] For example, the present intense activities focused on the realization of II-VI-based diode lasers involve II-VI ternaries and quaternaries with Mg as a constituent; the large band gaps of ternaries and quaternaries such as Zn-Mg-Se and Zn-Mn-S-Se have been exploited both for quantum confinement[2] as well as for achieving waveguide (cladding) structures.[4] In this context, the study of their basic physical properties such as band gap, lattice constant, and lattice dynamics has acquired special importance. Since Mg is much lighter than Hg, Cd, or Zn, the typical group II elements in the II-VI's, the incorporation of Mg in place of the heavier group II element results in an increase of the band gap as well as in lattice vibrational modes with frequencies significantly higher than those of the host II-VI semiconductor.

The relative masses of the constituent atoms in alloys and their interatomic force constants characterize the composition dependence of their zone-center optical phonon frequencies. In ternary alloys, their variation with composition can be categorized by one-mode, two-mode, and intermediate behavior.[5] For example, in $Cd_{1-y}Mn_yTe$, due to the significant mass difference between Cd and Mn, the optical phonons exhibit a two-mode behavior, whereas in $Zn_{1-y}Mn_yTe$, where masses of Zn and Mn are more closely matched, they show an intermediate behavior.[6] The zone-center optical phonons in $Cd_{1-x}Mg_xTe$ exhibit two-mode behavior, i.e., the local mode of Mg^{2+} in CdTe ($x \to 0$) evolves into MgTe-like LO and TO phonons with increasing x, and finally becomes the LO-TO modes of the the tetrahedrally coordinated (zinc-blende) MgTe; on the other hand, the CdTe LO and TO phonons converge into the Cd^{2+}-gap mode in MgTe with $x \to 1$.[1]

The physical properties of quaternary compounds are often of interest in the context of an additional control of material parameters such as band gap, lattice parameter, and valence band offsets in heterostructures. Lattice vibrations in some III-V quaternaries have already been reported in the literature.[7] We reported recently the vibrational modes of a II-VI-based quaternary, viz., $Cd_{1-x-y}Zn_xMn_yTe$ (Ref. 8), and showed that there are *three* longitudinal and transverse optical phonons, whose frequency variation with composition is similar to the intermediate behavior, exhibited, for example, by the ternary $Zn_{1-y}Mn_yTe$. In contrast, for $Cd_{1-x-y}Mg_xMn_yTe$ one expects an unambiguous three-mode (CdTe-like, MnTe-like, and MgTe-like modes) behavior, due to the distinct masses of the three kinds of cations. The Mg^{2+} local mode in $Cd_{1-y}Mn_yTe$ ($x \to 0$) should split into MgTe-like LO and TO phonons in the quaternary $Cd_{1-x-y}Mg_xMn_yTe$, and finally become the MgTe-LO and TO phonons in MgTe ($x \to 1$). Similarly, the Mn^{2+}-impurity mode in $Cd_{1-x}Mg_xTe$ ($y \to 0$) should evolve into the MnTe-LO and TO phonons in the zinc-blende MnTe ($y \to 1$), whereas the Cd^{2+}-gap mode in Mg_xMn_yTe ($x + y \to 1$) should become the CdTe-LO and TO phonons in CdTe.

In this paper, we present the results of a study on Raman scattering, band-gap photoluminescence, and infrared absorption spectroscopy in $Cd_{1-x}Mg_xTe$ and $Cd_{1-x-y}Mg_xMn_yTe$, motivated by the above considerations.

II. EXPERIMENTAL

The II-VI quaternaries and ternaries studied in the present investigation were grown by the modified Bridgman method. While CdTe, MnTe, and MgTe exhibit zinc-blende, NiAs, and wurtzite structure, respectively,

0163-1829/93/48(20)/15040(7)/$06.00

as an alloy $Cd_{1-x}Mg_xTe$ has a zinc-blende structure below x=0.6 and a wurtzite structure above it,[1] whereas $Cd_{1-y}Mn_yTe$ has zinc-blende structure for $0 \leq y \leq 0.77$. The composition was determined by electron microprobe analysis. The analysis in $Cd_{1-x}Mg_xTe$ showed that for most samples actual Mg concentrations were within ±5% of nominal concentrations, and in this paper we used nominal concentrations. Many of the samples were cleaved parallel to (110) and the cleaved surfaces were polished for backscattering measurement in the Raman scattering. For polishing samples with high Mg concentration, ethyl alcohol was used to prevent hydrolysis. In photoluminescence measurements, cleaved surfaces were used since it was found that the intensity was stronger for the cleaved surfaces than for those polished. Various excitation lines of a Kr^+ and an Ar^+ laser were used for exciting Raman and photoluminescence spectra. More detailed description of the experimental procedures for Raman scattering measurements is given in Ref. 8. For infrared absorption the samples were prepared with two plane parallel polished surfaces. The infrared absorption spectra were recorded using a BOMEM DA.3 Fourier-transform spectrometer and a composite silicon bolometer operating at 4.2 K.

III. RESULTS AND DISCUSSIONS

A. Band gap as a function of composition: Photoluminescence

In Fig. 1(a) we show the dependence of the band gap (E_g) of $Cd_{1-x}Mg_xTe$ at 10 K as a function of x, which yields $E_g = 1.595 + 1.607x$, whereas for $Cd_{1-y}Mn_yTe$, Lee, Ramdas, and Aggarwal[9] report $E_g = 1.595 + 1.592y$ at the same temperature. The extrapolation of the data yields E_g=3.20 eV for the *zinc-blende* MgTe. We note that Parker *et al.* have studied the band gap of $Zn_{1-x}Mg_xTe$, which has the zinc-blende structure for $x \leq 0.5$ and the wurtzite structure for $x \geq 0.5$.[10] From $E_g(x)$ for $x \geq 0.5$, deduced from band-edge luminescence produced by electron bombardment, they derived $E_g \sim 3.47$ eV for MgTe with the wurtzite structure; their data for $x \leq 0.5$, in which the alloy possesses a zinc-blende structure, yields for $x \to 1$, i.e., for zinc-blende MgTe, $E_g \sim 3.26$ eV.

The energy gap (E_g) of $Cd_{1-x-y}Mg_xMn_yTe$ as a function of x and y, determined from band-gap photoluminescence at 10 K is shown in Fig. 1(b). We studied a series of quaternaries for x=0.1, $x=y$, and y=0.1, corresponding to the dashed lines on the base, the solid squares representing the samples studied for photoluminescence. The data for $Cd_{1-y}Mn_yTe$ (x=0) are from Ref. 9. The values of E_g lie on a plane given by the equation

$$E_g = 1.595 + 1.607x + 1.592y. \quad (1)$$

For samples containing Mn, the photoluminescence observed at 2.03 ± 0.02 eV is due to the well-known $^6A_1(^6S) \to {}^4T_1(^4G)$ Mn^{2+} transition. There was no detectable dependence of the Mn^{2+} transition energy on Mg concentration and the transition energy agrees with previous photoluminescence measurements on $Cd_{1-y}Mn_yTe$.[11] For $E_g \geq 2.03$ eV, although the luminescence of the Mn^{2+} transition dominates, the band-gap luminescence is still observable.

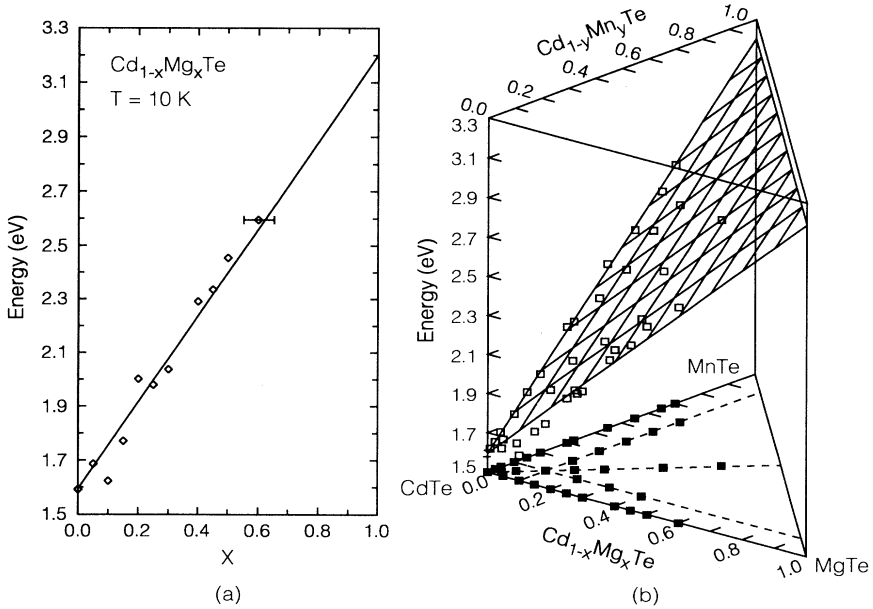

FIG. 1. (a) Energy gap of $Cd_{1-x}Mg_xTe$ as a function of x at T = 10 K. (b) Energy gap (E_g) of $Cd_{1-x-y}Mg_xMn_yTe$ as a function of Mg (x) and Mn (y) concentration, respectively. The solid squares on the basal triangle in (b) indicate Mg and Mn concentrations for the samples studied for the photoluminescence. The three dashed lines on the base correspond to x=0.1, $x = y$, and y=0.1. The open squares are the data for $E_g(x, y)$. The grid is the energy plane given by Eq. (1). Data along $x = 0$ is from Ref. 9.

B. Local modes of Mg^{2+}: Infrared absorption

Figure 2 shows the absorption spectrum of a CdTe sample doped with 10^{19} Mg/cm^3 in the range 125–320 cm^{-1} and of a $Cd_{0.95}Mg_{0.025}Mn_{0.025}Te$ sample in the range 340–600 cm^{-1}, the spectra being recorded at 4.75 K. For comparison, the absorption spectrum of pure CdTe is also shown. Three sharp features associated with the localized vibrations of the three Mg isotopes (^{24}Mg, ^{25}Mg, and ^{26}Mg) are clearly seen ~250 cm^{-1}, having intensities consistent with their natural abundances of 79%, 10%, and 11%, respectively. The second harmonics of these excitations are observed ~500 cm^{-1} in $Cd_{0.95}Mg_{0.025}Mn_{0.025}Te$. The Mn^{2+} local mode frequency in CdTe, deduced from Raman measurements,[12] is 195 cm^{-1} at 80 K; the intense reststrahlen band of CdTe precludes its direct observation in the infrared. However, its second harmonic is observed in $Cd_{0.95}Mg_{0.025}Mn_{0.025}Te$ at 380 cm^{-1}. In contrast to Mg, Mn has only one isotope (^{55}Mn) and correspondingly only a single local mode is seen.

Table I displays the isotopic masses, abundances, and the peak positions associated with the fundamentals and second harmonics of the local modes of Mg. Local modes of light impurities (S, Mg, Be) in $Cd_{1-x}Zn_xTe$ have been reported earlier[13] and the frequencies (ω_l) of different isotopes (for S and Mg) are given by $\omega_l = (f/M_i)^{1/2}$, where M_i is the mass of the light impurity and f is the effective force constant for the impurity. The present observations on the local modes of Mg in CdTe confirm this quadratic dependence on the isotopic mass. Note that due to anharmonicity, the frequency of the first overtone is slightly less than twice that of the fundamental.

C. Lattice vibrations in $Cd_{1-x}Mg_xTe$

Figure 3 shows the Raman spectrum of $Cd_{1-x}Mg_xTe$, x=0.2 at T=10 K with excitation wavelength λ_L=6471 Å. The peaks at 260 cm^{-1} and 168 cm^{-1}, labeled ω_1 and ω_2, correspond to the MgTe-like and CdTe-like LO phonons, respectively. The background underlying the Raman lines is due to the tail of a photoluminescence band. Overtones up to $5\omega_2$ as well as the combinations of ω_1 and ω_2 can be seen under the strong "out" resonance condition fulfilled in the experiment.

We note here that, in addition to the CdTe-like and MgTe-like zone-center optical phonons, there are weak features at ~ 225 cm^{-1} and 247 cm^{-1}, labeled a and b on the lower energy side of ω_1. With λ_L=6764 Å, we observed weak signatures at ~ 145.5 cm^{-1} and 156 cm^{-1}, labeled c and d in the inset of the figure. Nakashima

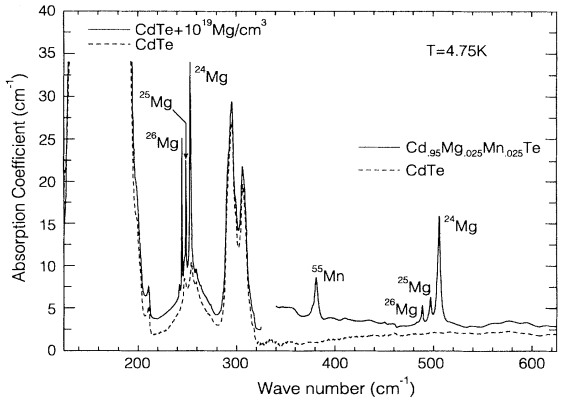

FIG. 2. The infrared absorption spectra for a CdTe sample doped with 10^{19} Mg/cm^3 (125–320 cm^{-1}) and $Cd_{0.95}Mg_{0.025}Mn_{0.025}Te$ (340 – 600 cm^{-1}) (solid curves) at 4.75 K. For comparison, a spectrum of pure CdTe is shown at the same temperature with a dashed curve and shifted down by 2.5 cm^{-1} for clarity. The peaks associated with the fundamentals and the second harmonics of the local modes of the three Mg isotopes (^{24}Mg, ^{25}Mg, and ^{26}Mg) as well as the second harmonic of the Mn^{2+} local mode are clearly seen in the figure.

et al.,[1] on the basis of x-ray analysis, reported that $Cd_{1-x}Mg_xTe$ in the range $0.3 \leq x \leq 0.6$ contains domains of $6H$ polytype. As in the $6H$ polytype of SiC (Ref. 14), one expects the transitional period along [111] to become six times larger compared to that in the zinc-blende structure, resulting in a correspondingly smaller Brillouin zone. Assuming crystal field splitting to be negligible, one can visualize zone folding of the optical branch, making phonons at $q = 1/3$ and $q = 2/3$ (in units of q_{max}, q_{max} being the maximum wave vector along [111] for the zinc-blende structure) occur at the zone center of the reduced Brillouin zone and hence Raman active, in addition to the $q = 0$ phonons. Although x=0.2 is somewhat smaller than the lower limit of the range claimed for the occurrence of a $6H$ polytype, it is tempting to attribute these signatures to the presence of small domains with $6H$ structure, the peaks b and a being MgTe-like LO phonons at $q = 1/3$ and $2/3$, respectively, and the peaks d and c being the CdTe-like LO phonons at $q = 1/3$ and $2/3$, respectively. The combination modes of MgTe-like LO phonons at $q = 1/3$ and $2/3$, i.e., of b and a with the CdTe-like LO at $q = 0$, appear on the lower energy side of $\omega_1 + \omega_2$, at ~390 cm^{-1} and 415 cm^{-1} and the combination modes of CdTe-like LO phonons at $q = 1/3$ and $2/3$, i.e., of d and c with the $q = 0$ CdTe LO, appear at ~324 cm^{-1} and 313.5 cm^{-1}, on the lower energy side

TABLE I. Local mode frequencies for the three isotopes of Mg^{2+} at T~5 K.

Atomic mass	Abundance (%)	Fundamental (cm^{-1})	Second harmonic (cm^{-1})
23.985	78.99	253.3	505.3
24.986	10.00	248.8	496.4
25.983	11.01	244.7	488.2

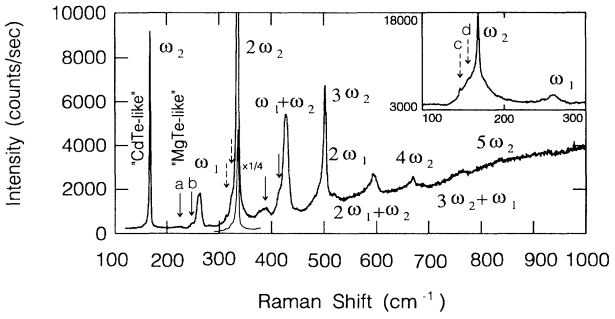

FIG. 3. Raman spectrum of $Cd_{1-x}Mg_xTe$, x=0.2, at T = 10 K excited with the Kr^+ line λ_L=6471 Å. The Raman lines labeled ω_1 and ω_2 correspond to the MgTe-like and CdTe-like LO phonons, respectively. The weak features identified with arrows (a and b) are ascribed to the optical phonons arising from domains of 6H structure (see text). The inset shows the Raman spectrum excited with λ_L= 6764 Å, where ω_2 has been further enhanced due to resonance conditions more closely fulfilled; c and d are attributed to 6H domains.

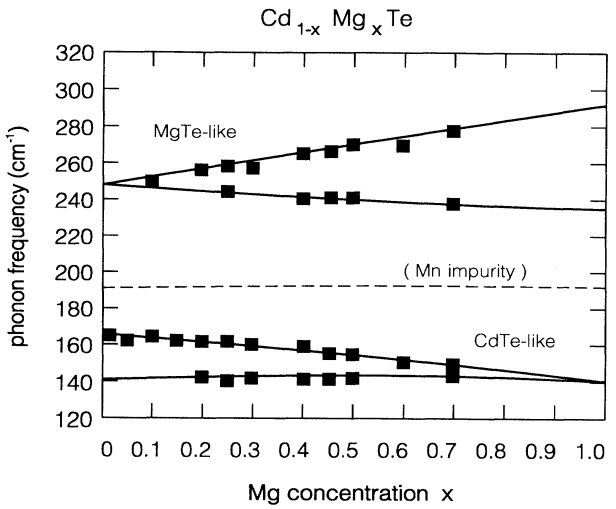

FIG. 4. The zone-center optical phonons of $Cd_{1-x}Mg_xTe$ as a function of x at 300 K, showing a two-mode behavior. The dashed line shows the Mn-impurity mode in $Cd_{1-x}Mg_xTe$.

of $2\omega_2$; all four have been indicated with arrows.

The optical phonon frequencies in $Cd_{1-x}Mg_xTe$ at room temperature as a function of x is shown in Fig. 4, where the MgTe-like and CdTe-like modes have been identified. We note here that we often observe an unidentified peak in the range 183–200 cm^{-1} for $Cd_{1-x}Mg_xTe$ with $x \geq 0.2$. The curves in the figure are theoretical fits to the data by using the modified random isodisplacement (MREI) model[15] with the fitting parameters shown in Table II. The dashed curve shows the Mn-impurity mode as a function of Mg concentration, for comparison with MnTe-like phonon frequencies in $Cd_{1-x-y}Mg_xMn_yTe$, which will be discussed later. The local mode of Mg^{2+} in CdTe obtained from an extrapolation of the fit is 248 cm^{-1} at room temperature and 253 cm^{-1} at 10 K. Note that in the infrared absorption measurements with a lower concentration of Mg, we observe three peaks due to *local* modes of the Mg isotopes, whereas in the Raman measurements with $x \geq 0.05$, we observe the *collective* motion of Mg atoms, i.e., MgTe-like phonons. The weighted average of the local mode frequencies of Mg isotopes is 252 cm^{-1} at 5 K, close to the impurity mode frequency obtained from the MREI model fitting at 10 K. In Ref. 1 the LO phonon frequency of zinc-blende MgTe obtained by extrapolation to x=1 is 320 cm^{-1}, significantly higher than our value of 292 cm^{-1}, both being estimated at room temperature. Another feature of the MREI fit is the value of the static dielectric constant (ϵ_o) of zinc-blende MgTe—here we use ϵ_o=7.01, which is the quoted value for wurtzite MgTe.[16] No evidence of the crystal field splittings expected for x≥0.6 for the wurtzite structure appears for the phonon features in $Cd_{0.3}Mg_{0.7}Te$.

D. Three-mode behavior in $Cd_{1-x-y}Mg_xMn_yTe$

The Raman spectra for $Cd_{1-x-y}Mg_xMn_yTe$ with x=y=0.2 and 0.3, the former in the backscattering and the latter in the right angle scattering geometry, with λ_L=6471 Å, are shown in Fig. 5.

In both spectra, two peaks around 44 cm^{-1} and 116

TABLE II. Parameters in the MREI model for $Cd_{1-x-y}Mg_xMn_yTe$ (T=300 K). Lattice parameter $a = 6.486 - 0.386x - 0.145y$ (Å). Lattice constant of MgTe, not available at present, is obtained as a fitting parameter. Parameters for force constants [in units of 10^6 amu cm^{-2}]: F_{Cd-Te}=1.68, F_{Mg-Te}=1.37, F_{Mn-Te}=1.62, F_{Cd-Mg}=0.25, F_{Cd-Mn}=0.56, F_{Mg-Mn}=0.17, and Θ=3.5, where F and Θ are defined by $f = F\{1 + \Theta[a(\text{MnTe}) - a]/a(\text{MnTe})\}$, f being the force constant for the quaternary.

CdTe	MgTe	MnTe
ω_{TO}(CdTe)=141 cm^{-1}	ω_{TO}(MgTe)=235 cm^{-1}	ω_{TO}(MnTe)=180 cm^{-1}
ω_{LO}(CdTe)=166 cm^{-1}	ω_{LO}(MgTe)=292 cm^{-1}	ω_{LO}(MnTe)=211 cm^{-1}
ω_I(CdTe:Mg)=248 cm^{-1}	ω_I(MgTe:Cd)=140 cm^{-1}	ω_I(MnTe:Cd)=141 cm^{-1}
ω_I(CdTe:Mn)=191 cm^{-1}	ω_I(MgTe:Mn)=192 cm^{-1}	ω_I(MnTe:Mg)=252 cm^{-1}
ϵ_o(CdTe)=9.6	ϵ_o(MgTe)=7.0	ϵ_o(MnTe)=11.0

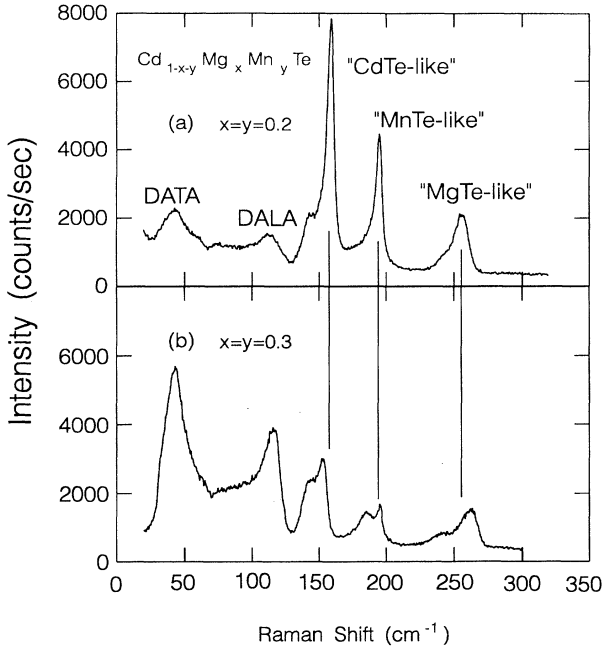

FIG. 5. Raman spectra for $Cd_{1-x-y}Mg_xMn_yTe$, (a) $x=y=0.2$ in the backscattering geometry and (b) $x=y=0.3$, with right angle scattering geometry, $\lambda_L=6471$ Å, $T = 300$ K. Three pairs of optical phonons (CdTe-like, MnTe-like, and MgTe-like) and the disorder-actived transverse and longitudinal acoustic (DATA and DALA) phonon features are indicated in the figure.

cm^{-1} are clearly observed. The frequencies are almost identical with peak frequencies of the features of the Raman spectra in this spectral range observed for ternary and quaternary alloys, e.g., $Cd_{1-x-y}Zn_xMn_yTe$, and attributed to the disorder-activated transverse and longitudinal acoustic phonons (DATA and DALA). This assignment is based on the similarity of the one-phonon density of states and the line shape in the Raman spectrum, especially the asymmetry of the DALA line.[12]

On the basis of the Raman spectra of CdTe, $Cd_{1-y}Mn_yTe$, and $Cd_{1-x}Mg_xTe$, the three peaks associated with optical phonons are identified as CdTe-like, MnTe-like, and MgTe-like LO phonons.

As in $Cd_{1-x-y}Zn_xMn_yTe$, the composition dependence of zone-center optical phonons in quaternaries can be readily understood from the MREI model, where one assumes that same kinds of atoms vibrate with same amplitude and phase in the long-wavelength limit and that the restoring forces acting on each atom are given by the statistical averages of the interatomic forces between neighboring atoms.[15] In the model, the interatomic forces and forces due to the local electric field in a given alloy can be deduced from the macroscopic parameters characterizing the end binary members, such as dielectric constants and transverse optical phonon frequencies, by a linear interpolation. The end binary members for $Cd_{1-x-y}Mg_xMn_yTe$ with their macroscopic parameters are shown in Table II.

A complete picture of the zone-center optical phonons for the quaternaries is represented in Fig. 6. The points inside the basal triangle represent the quaternaries of different compositions, above which the corresponding six phonon frequencies (three LO and three TO frequencies) are plotted on a vertical scale. The phonon frequencies as a function of composition (x and y) form surfaces, labeled LO_1, TO_1, LO_2, TO_2, LO_3, and TO_3 from the top, the frequencies being generated by the MREI model. As expected on the basis of the atomic masses, the MgTe-like modes have the highest frequencies and CdTe-like modes the lowest frequencies. In the figure, the solid curves show CdTe-like and MnTe-like phonon frequencies in $Cd_{1-y}Mn_yTe$ as well as the local mode of Mg represented by the intersection of the LO_1 and TO_1 phonon surfaces.

Two cross sections of Fig. 6 are shown in Fig. 7, viz., for $x=y$ (a) and for $x=0.1$ (b). The squares are the data values obtained at room temperature from raw data such as those displayed in Fig. 5 and the solid lines are the theoretical fits.[17]

The force constants in Te-based II-VI semiconductors, used for the MREI model, appear to show a consistent variation with the masses of cations. In order to compare the force constants with the same interatomic distance, we choose the force constant F in the zinc-blende MnTe, F being defined by the force constant f in $f = F\{1 + \Theta[a(\text{MnTe}) - a]/a(\text{MnTe})\}$. The MREI fits yield $F_{\text{Cd-Zn}}=0.54$, $F_{\text{Cd-Mn}}=0.56$, $F_{\text{Zn-Mn}}=0.38$, $F_{\text{Cd-Mg}}=0.25$, $F_{\text{Mg-Mn}}=0.17$ ($\times 10^6$ amu cm^{-2}) from the data for $Cd_{1-y}Mn_yTe$, $Zn_{1-y}Mn_yTe$, $Cd_{1-x}Mg_xTe$, and $Cd_{1-x-y}Mg_xMn_yTe$, whereas for the nearest neighbor interaction between cation and Te, one obtains $F_{\text{Cd}}=1.68$,

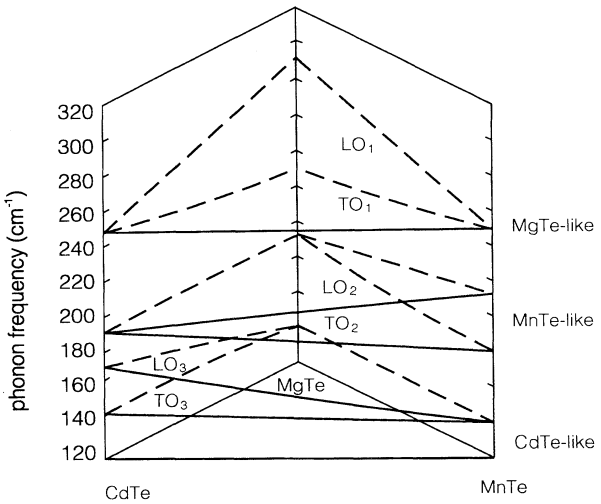

FIG. 6. The zone-center optical phonons of the quaternary $Cd_{1-x-y}Mg_xMn_yTe$. The solid curves represent optical phonons in $Cd_{1-y}Mn_yTe$ and dashed ones represent those for $Cd_{1-x}Mg_xTe$ and Mg_xMn_yTe. The six surfaces (labeled LO_1, TO_1, LO_2, TO_2, LO_3, and TO_3) circumscribed by the solid and dashed curves represent three (MgTe-like, MnTe-like, and CdTe-like) LO-TO pairs.

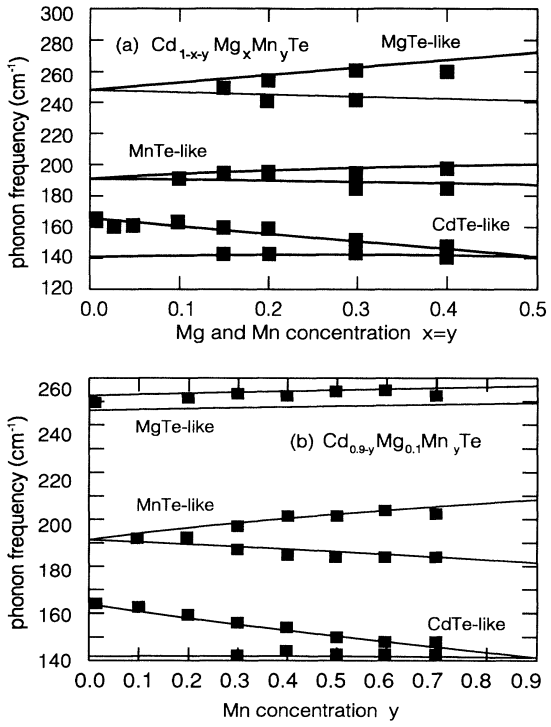

FIG. 7. The composition dependence of zone-center optical phonons in $Cd_{1-x-y}Mg_xMn_yTe$, (a) $x=y$ and (b) $x=0.1$. The solid curves are generated from the MREI model with fitting parameters given in Table II.

$F_{Zn}=1.49$, $F_{Mn}=1.62$, and $F_{Mg}=1.37$ ($\times 10^6$ amu cm^{-2}); all the values are deduced from room temperature data. Note that the force constant due to overlap potential is larger between heavier (or larger) atoms, as expected, except the order is reversed for Zn and Mn, where the masses of the two atoms are close. A similar dependence of the force constant on the ionic radius was reported earlier by Harada and Narita,[13] who obtained force constants both from the local modes of Be and Mg in CdTe and from the reststrahlen reflectivity of $Cd_{1-x}Zn_xTe$ and showed that a log-log plot of force constant vs ionic radius is linear.

We note here that the LO phonon lines have lower energy tails, as can be seen in Fig. 5. Such an asymmetry in the LO phonon lines has been reported in $Ga_{1-x}Al_xAs$,[18,19] in ZnS_xSe_{1-x},[20] and in $Cd_{1-x}Zn_xTe$.[21] Differing mechanisms have been proposed for the origin of this asymmetry, viz., relaxation of the q-vector conservation in a disordered system[18–20,22] or a Fano-type interaction.[21] We have yet to carry out a quantitative analysis of this asymmetry in the context of these alternative models.

IV. CONCLUDING REMARKS

In the present study we have demonstrated that the infrared and Raman spectra of the II-VI ternary and quaternary alloys provide excellent illustrations of a local mode in a binary evolving into collective LO and TO modes, which extrapolate to the corresponding LO and TO modes of other binaries involved in the alloy. Thus, $Cd_{1-x-y}Mg_xMn_yTe$ displays a characteristic three-mode behavior with CdTe-like, MnTe-like, and MgTe-like LO-TO pairs. While the Raman spectra allow the observation of the multimode behavior over a large composition range and permit the *inference* of the local mode frequency from an extrapolation of the data to extremely high dilutions of the relevant constituent (for example, Mg in CdTe), such a local mode can be *directly* observed in the infrared; when thus observed, the frequency shift of the local mode with isotopic mass is unmistakably manifested. As the concentration increases, the *local* mode transforms into a *collective* mode and the isotopic dependence is obliterated, to be replaced by average mass, as visualized in the virtual crystal approximation. Our study emphasizes the advantages of exploiting the complementary features of infrared and Raman spectroscopy. Of course, the study of the reststrahlen spectra of the ternaries and quaternaries can, in principle, yield the composition dependence of the LO and TO frequencies over the entire composition range. However, this has to be deduced indirectly from the theoretical fits of the dielectric function to the reststrahlen spectra, whereas the LO and TO modes appear in the Raman spectra as distinct lines with spectroscopic accuracy. Finally, the Raman spectra of ternaries and quaternaries allow one to deduce LO-TO frequencies of metastable binary end members such as MnTe and MgTe, with zinc-blende structure. It has been recently shown that these metastable zinc-blende structures can be grown by molecular beam epitaxy, as has been shown for MnTe and MnSe;[23] the LO phonons of zinc-blende MnTe (Ref. 24) and MnSe (Ref. 25) thus grown have been reported in the literature.

As is well known, the presence of a transition metal ion, e.g., Mn^{2+}, results in pronounced magnetic properties due to the large spin-spin exchange interaction between the band electrons and the transition metal ions (the so-called *sp-d* exchange interaction). For example, these interactions lead to huge Zeeman splittings of the interband transitions, resulting in a large redshift of the band gap photoluminescence and giant magneto-optic effects.[26] Indeed, in $Cd_{1-x-y}Mg_xMn_yTe$, we observe magnetic characteristics similar to ternary diluted magnetic semiconductors, i.e., the large redshift of the band-gap photoluminescence and the Raman electron paramagnetic resonance of Mn^{2+}.

ACKNOWLEDGMENT

This research was supported by National Science Foundation Grant No. DMR-92-21390.

[1] S. Nakashima, T. Fukumoto, A. Mitsuishi, and K. Itoh, J. Phys. Soc. Jpn. **35**, 1437 (1973).
[2] H. Okuyama, F. Hiei, and K. Akimoto, Jpn. J. Appl. Phys. **31**, L340 (1992).
[3] M. C. Phillips, M. W. Wang, J. F. Swenberg, J. O. McCaldin, and T. C. McGill, Appl. Phys. Lett. **61**, 1962 (1992).
[4] D. C. Grillo, Y. Fan, J. Han, L. He, R. L. Gunshor, A. Salokatve, M. Hagerott, H. Jeon, A. V. Nurmikko, G. C. Hua, and N. Otsuka, Appl. Phys. Lett. (to be published).
[5] A. S. Barker, Jr. and A. J. Sievers, Rev. Mod. Phys. **47**, S1 (1975).
[6] D. L. Peterson, A. Petrou, W. Giriat, A. K. Ramdas, and S. Rodriguez, Phys. Rev. B **33**, 1160 (1986).
[7] See, for example, in In-Ga-As-P, A. Pinczuk, J. M. Worlock, R. E. Nahory, and M. A. Pollack, Appl. Phys. Lett. **33**, 461 (1992).
[8] E. Oh, R. G. Alonso, I. Miotkowski, and A. K. Ramdas, Phys. Rev. B **45**, 10 934 (1992).
[9] Y. R. Lee, A. K. Ramdas, and R. L. Aggarwal, Phys. Rev. B **38**, 10 600 (1988).
[10] S. G. Parker, A. R. Reinberg, J. E. Pinnell, and W. C. Holton, J. Electrochem. Soc. **118**, 979 (1971).
[11] R. Y. Tao, M. M. Moriwaki, W. M. Becker, and R. R. Galazka, J. Appl. Phys. **53**, 3772 (1982).
[12] S. Venugopalan, A. Petrou, R. R. Galazka, A. K. Ramdas, and S. Rodriguez, Phys. Rev. B **25**, 2681 (1982).
[13] H. Harada and S. Narita, J. Phys. Soc. Jpn. **30**, 1628 (1971).
[14] D. W. Feldman, J. H. Parker, Jr., W. J. Chyke, and L. Patrick, Phys. Rev. **170**, 698 (1968).
[15] L. Genzel, T. P. Martin, and C. H. Perry, Phys. Status Solidi B **62**, 83 (1974); I. F. Chang and S. S. Mitra, Phys. Rev. **172**, 924 (1968).
[16] See J. A. van Vechten, Phys. Rev. **182**, 891 (1969).
[17] In the microprobe measurements, we found that Mg concentrations were often lower than the nominal concentrations, whereas Mn concentrations were close to the nominal concentrations. The biggest difference was observed for the nominal concentrations of $x=y=0.4$, where the microprobe results give $x=0.31$ and $y=0.43$.
[18] J. Shah, A. E. DiGiovanni, T. C. Damen, and B. I. Miller, Phys. Rev. B **7**, 3481 (1973).
[19] B. Jusserand and J. Sapriel, Phys. Rev. B **24**, 7194 (1981).
[20] K. Hayashi, N. Sawaki, and I. Akasaki, Jpn. J. Appl. Phys. **30**, 501 (1991).
[21] D. J. Olego, P. M. Raccah, and P. Faurie, Phys. Rev. B **33**, 3819 (1986).
[22] P. Parayanthal and F. H. Pollak, Phys. Rev. Lett. **52**, 1822 (1984).
[23] R. L. Gunshor, in *Strained-layer Superlattices: Materials Science and Technology*, edited by T. P. Pearsall, Vol. 33 Semiconductors and Semimetals (Academic Press, New York, 1991), Chap. 6, p. 337.
[24] N. Pelekanos, Q. Fu, J. Ding, W. Walecki, A. V. Nurmikko, S. M. Durbin, J. Han, M. Kobayashi, and R. L. Gunshor, Phys. Rev. B **41**, 9966 (1990).
[25] E. Oh, A. K. Ramdas, N. Samarth, H. Luo, and J. K. Furdyna, Phys. Rev. B **47**, 7288 (1993).
[26] See, for example, A. K. Ramdas and S. Rodriguez, in *Light Scattering in Solids VI*, edited by M. Cardona and G. Güntherodt (Springer-Verlag, New York, 1991), p. 137.